Medical display application for degraded image sharpness restoration based on the modulation transfer function: Initial assessment for a five-megapixel mammography display monitor

Tokurei, Shogo
Department of Radiological Science, Faculty of Health Sciences, Junshin Gakuen University

Ikushima, Yoichiro
Department of Radiological Science, Faculty of Health Sciences, Junshin Gakuen University

Takegami, Kazuki
Department of Radiological Technology, Yamaguchi University Hospital

Okada, Munemasa
Department of Radiology, Yamaguchi University Graduate School of Medicine

他

出版情報：Physical and Engineering Sciences in Medicine. 44 (2), pp.581-589, 2021-06-01. Springer
バージョン：
権利関係：

Title

Medical display application for degraded image sharpness restoration based on the modulation transfer function: Initial assessment for a five-megapixel mammography display monitor

Author Names

Shogo Tokurei 1, Yoichiro Ikushima 1, 2, Kazuki Takegami 3, 4, Munemasa Okada 5, Junji Morishita 6

Affiliations

1. Department of Radiological Science, Faculty of Health Sciences, Junshin Gakuen University, 1-1-1 Chikushigaoka, Minami-ku, Fukuoka 815-8510, Japan

2. Department of Health Sciences, Graduate School of Medical Sciences, Kyushu University, 3-1-1 Maidashi, Higashi-ku, Fukuoka 812-8582, Japan

3. Department of Radiological Technology, Yamaguchi University Hospital, 1-1-1 Minamikogushi, Ube, Yamaguchi 755-8505, Japan

4. Division of Health Sciences, Graduate School of Medical Sciences, Kanazawa University, 5-11-80 Kodatsuno, Kanazawa, Ishikawa, 920-0942, Japan

5. Department of Radiology, Yamaguchi University Graduate School of Medicine, 1-1-1 Minamikogushi, Ube, Yamaguchi 755-8505, Japan

6. Department of Health Sciences, Faculty of Medical Sciences, Kyushu University, 3-1-1 Maidashi, Higashi-ku, Fukuoka 812-8582, Japan

Corresponding Author details

Shogo Tokurei R.T., Ph.D.
E-mail: stokurei@junshin-u.ac.jp
Telephone number: +81-92-554-1255
Fax number: +81-92-551-0072
ORCID: 0000-0002-3240-7732

Abstract

An image-display application for medical liquid-crystal display (LCD) monitors called the sharpness recovery (SR) function has been developed to compensate for image sharpness as a function of deficiencies in the modulation transfer function (MTF) of a monitor. We investigated the effects of the SR function for a five-megapixel (MP) mammography LCD monitor on the resolution and noise properties of the displayed images by measuring the MTF and overall noise power spectrum (NPS), respectively. Furthermore, the effectiveness of the SR function for the 5-MP monitor in displaying subtle microcalcifications on digital mammograms was verified using a two-alternative-forced-choice sensitivity measurement as an initial application for medical image interpretation. Four radiologists compared the visibility of 45 regions of interest with a malignant microcalcification cluster shown on SR-processed and unprocessed mammograms. SR processing improved the MTF of the displayed images by approximately 40% at the Nyquist frequency of the 5-MP monitor, whereas it slightly increased the overall NPS values. All observers indicated that the

fraction of cases considered to have better visibility of microcalcifications with the SR processing was significantly greater than that without the processing (averaging 82%, with the 95% confidence interval ranging from 70 to 93%). The SR processing for the 5-MP monitor yielded a significant improvement in the resolution properties of the displayed images, with a certain increase in the image noise. The SR function has the potential to improve the observer performance of radiologists, particularly when reading subtle microcalcifications reproduced on 5-MP monitors.

Keywords: liquid-crystal display monitor, image sharpness, modulation transfer function, image processing, digital mammography, two-alternative-forced-choice sensitivity measurement

1 Introduction

Ideally, diagnostic soft-copy displays, such as cathode ray tubes (CRTs) and liquid-crystal display (LCD) monitors, should be able to represent digital radiographic images without any loss in the characteristics of the original image captured by computed radiography and flat-panel detector (FPD) systems. However, the perceived quality of the final displayed medical image on the monitor is influenced by the inherent physical properties and characteristics of the monitor [1, 2]. The resolution properties of LCD monitors, which represent the ability of a display to reproduce the spatial details of an image, are limited by the inherent characteristics of the display such as the pixel size, surface treatment, aperture ratio of the display panel, and color filter on a color monitor [3–6]. The final displayed images on the LCD monitor are degraded in terms of image sharpness because of the resolution limit of the display device [7]. The degradation in the image sharpness can be characterized by the modulation transfer function (MTF) of the LCD monitor (hereinafter referred to as monitor MTF). In particular, the fraction of the total pixel area that allows transmission of lights in a display panel (called the pixel aperture ratio) designed for a five-megapixel (MP) mammography display monitor has been recently increased to achieve higher brightness, such as 2,000–2500 cd/m^2, than that of a conventional mammography display (Fig. 1), thereby causing a degradation in the monitor's MTF.

The post-processing of digital images can help improve the diagnostic performance of soft-copy reading [8, 9]. In previous studies, it was shown that the post-processing performed to compensate for the MTF deficiencies in conventional CRT monitors can improve soft-copy presentation for chest radiographs and mammograms [10-13]. Recently, a display application for medical LCD monitors called the sharpness recovery (SR) function was developed to compensate for image sharpness in real time as a function of the deficiencies in the monitor's MTF. According to the White Paper, the SR application led to a slight improvement in the diagnostic accuracy or reader efficiency of bone fracture images for a 3-MP LCD monitor [14]. The SR function is an image-space filtering technique aimed at enhancing the sharpness of medical images with high spatial frequency signals, such as microcalcifications on digital mammograms. Sivaramakrishna et al. [8] showed that mammographic image enhancement algorithms, such as unsharp masking, histogram equalization, region-based or adaptive neighborhood enhancement, and wavelet, appear to improve the visibility of clustered microcalcifications. In this study, we verified the effects of this SR function for a 5-MP mammography LCD monitor on the resolution and noise properties of the displayed images by measuring the MTF and noise power spectrum (NPS), respectively. Furthermore, we demonstrated the effectiveness of the SR function in displaying subtle microcalcifications on digital mammograms using a two-alternative-forced-choice (2-AFC) method as an initial application for the 5-MP mammography LCD monitor.

2 Methods

2.1 LCD Monitor and Mammography Equipment

The display devices equipped with the SR function were two 5-MP monochrome mammography LCD monitors with an anti-glare panel (RadiForce GX550, EIZO Corporation, Ishikawa, Japan) comprising 2,048 × 2,560 pixels with a pixel pitch of 165 μm × 165 μm. The brightness of the two LCD monitors was calibrated at a maximum luminance of

600 cd/m^2. The display functions of the two LCD monitors were set to the grayscale standard display function (GSDF). We preliminarily confirmed that the two LCD monitors used for our 2-AFC study were comparable in terms of their inherent MTF and NPS characteristics. The inherent MTFs and NPS of the 5-MP LCD monitors were measured using a commercially available single-lens reflex digital camera (resolution: 5,472 × 3,648 pixels; EOS 6D, Canon, Tokyo, Japan) equipped with a close-up lens (MACRO 70mm F2.8 EX DG, SIGMA Co. Kanagawa, Japan) in a dark room, as presented in Ref. [6]. The monitor MTFs were determined based on the line responses, which were acquired from the captured image of a horizontal or vertical 1-pixel line pattern. Figure 2(a) shows that the monitor MTFs have anisotropic properties in the horizontal and vertical directions because of the pixel structure of the LCD monitors [6]. The inherent NPS of the LCD monitors were measured from the one-dimensional (1-D) noise profiles, which were obtained by scanning the captured images of a uniform test pattern with a 100% digital drive level (DDL) using a numerical slit. As shown in Fig. 2(b), the inherent NPS of the LCD monitors suggests little difference in the noise level owing to the luminance fluctuations in the pixels between the horizontal and vertical directions.

To acquire phantom and mammographic images, we used AMULET Innovality (Fujifilm Corporation, Tokyo, Japan), which is a full-field digital mammography imaging system, built from a direct-conversion FPD panel comprising 3,540 × 4,740 pixels with a pixel pitch of 50 μm × 50 μm.

2.2 Sharpness Recovery Function

The display application for the SR function was designed to restore the modulation transfer losses in the LCD monitor, and thus improve the sharpness of the displayed images in real time [10-14]. As the display functions of LCD monitors are expressed in terms of the luminance value–digital driving level curve, the digital image data were converted into luminance data and then processed using the SR-processing algorithm described below. When a digital image was displayed on the LCD monitor, the original image data in the frequency domain F (u, v) were modulated and blurred by the monitor MTF $MTF_{monitor}$ (u, v). The deteriorated image data G (u, v) can be processed with the inverse of the monitor MTF, acting as an inverse filter, to restore the image sharpness when reproduced on the LCD monitor. If the effect of image noise is neglected, the compensated image data G' (u, v), which is now theoretically equivalent to the original image data F (u, v), can be reconstructed as follows:

$$G'(u, v) = G(u, v) \times \frac{1}{MTF_{monitor}(u, v)} = (F(u, v) \times MTF_{monitor}(u, v)) \times \frac{1}{MTF_{monitor}(u, v)}. \quad (1)$$

The finite impulse response (FIR) inverse filter was calculated by taking the inverse Fourier transform (denoted by F^{-1}) of the desired frequency response obtained from the inverse of the monitor MTFs [15]. The compensated image data g' (x, y) in the real domain can be derived by simply convolving the displayed image data g (x, y) with the inverse filter coefficients:

$$g'(x, y) = g(x, y) * F^{-1}\left[\frac{1}{MTF_{monitor}(u, v)}\right]. \quad (2)$$

The inverse filter coefficients built in the present SR application were restricted to a matrix of size 5 × 5 to optimize the SR-processing algorithm for real-time implementation on medical workstations; this restriction of filter size led to deviations from the ideal frequency responses representing the inverse of the monitor MTFs. In this study, the frequency responses of the inverse filters, whose coefficients were approximated with a restricted size of 3 × 3, 5 × 5, and 7 × 7, were computed to demonstrate the capability of representing the ideal responses of the inverse monitor MTFs.

2.3 Physical Evaluations

The sharpness enhancement effects of the SR function on the final displayed images were determined based on the MTF measurement using a bar-pattern method proposed by Ichikawa et al. [16]. The test pattern consisted of five

segments, including the five bars with 1-, 2-, 3-, 4-, and 6-pixel widths, which corresponded to approximately 3.0, 1.5, 1.0, 0.76, 0.5 cycles/mm for the 5-MP monitor, respectively. In this study, the bar pattern with 50%-DDL bars on a 25%-DDL background area was acquired using a digital camera with a close-up lens. The square-wave profiles induced by the SR function were obtained from one-dimensional (1-D) profiles across the bar pattern. The MTF with the SR function was calculated from the amplitude of the fundamental frequency components extracted from the square-wave profiles using Fourier transformation.

The effects of the SR function on the overall NPS of the displayed image were measured using the luminance distributions of the LCD monitor on which an X-ray phantom image was reproduced, adopting the same calculation method as that for the inherent NPS of the LCD monitor [5, 17]. In this study, an American College of Radiology (ACR) accreditation phantom was imaged using the digital mammography system described by Ichikawa et al. [17]. The exposure conditions were selected as 28 kVp and 64.7 mAs, with a W/Rh anode-filter combination. The uniform area between test objects, such as simulated fibers and masses, in the ACR phantom image was acquired using a digital camera with a close-up lens. The display magnification of the ACR phantom image was set at a pixel-by-pixel size. The 1-D noise profiles were extracted by scanning the uniform area of the ACR phantom image with a numerically synthesized slit that had a width equal to the display-pixel size. The overall NPS was computed by considering the Fourier transforms of the 1-D noise profiles [6].

2.4 Observer Performance Study

This retrospective observation study was approved by our institutional review board, and an informed consent requirement was waived. We performed a 2-AFC sensitivity measurement (2-AFCSM) to determine the effectiveness of the SR function in improving the visibility of subtle microcalcifications on digital mammograms [18]. Four radiologists with 4–6 years of experience participated in the 2-AFCSM. The cases were acquired with the digital mammography system at Yamaguchi University Hospital between April and November 2016. A set of 45 craniocaudal or mediolateral view digital mammograms were selected by experienced mammographers who did not participate in the observer performance experiments. Each single view contained a circular region of interest (ROI) with one cluster of malignant microcalcifications, which were considered very subtle or extremely subtle for visual detection. The digital mammographic images were reduced to their life sizes using bilinear interpolation [19]; this size corresponds to a resampling scale factor of approximately 0.303. This life-size magnification ratio is used when bilateral breast images are displayed side-by-side on the 5-MP LCD screen for the initial representation on a diagnostic viewer [5]. Each pair of the same images randomly generated with and without the SR processing was shown to the radiologists on the two LCD monitors side-by-side. The radiologists were asked to choose between the two ROIs with better visibility in interpreting the clustered microcalcifications in a dark room. In this 2-AFCSM, the number of SR-processed images judged to have better visibility (i.e., true positive fraction) became equal to that of the unprocessed images judged not to have better visibility (i.e., true negative fraction). Windowing or zooming functions were not permitted to maintain consistent experimental conditions.

The effectiveness of the SR function in improving the visibility of subtle microcalcifications was evaluated in terms of the average percentage of the number of SR-processed images judged to have better visibility and the 95% confidence interval (CI) of the average for four observers. A binomial test was used to evaluate the significance of the differences between SR-processed and unprocessed mammographic images in interpreting the clustered microcalcifications. A statistically significant p-value was set to be less than 0.05. All statistical analyses were performed using the open-source R software (version 4.0.3; R Foundation for Statistical Computing, Vienna, Austria).

3 Results

Table 1 shows the filter coefficients with a restricted size of 5 × 5 used in this study, which were calculated from the inverse of the measured MTFs in the horizontal and vertical directions of the 5-MP mammography LCD monitor. Figure 3 shows comparisons of the frequency response functions in the horizontal and vertical directions, between the inverse of the measured MTFs and the inverse filters with restricted sizes of 3 × 3, 5 × 5, and 7 × 7. The 7 × 7 filter coefficients were able to represent the nearest frequency response to the inverse of the monitor MTFs in the horizontal and vertical directions, followed by 5 × 5 filter coefficients (for SR function), and 3 × 3 filter coefficients.

Figure 4 presents the square-wave profiles and MTFs in the horizontal and vertical directions, as measured from the SR-processed and unprocessed bar-pattern images reproduced on the 5-MP LCD monitor, respectively. The edge enhancements (overshoot and undershoot) induced by the SR function were visible on the square-wave profiles. The MTFs in the horizontal and vertical directions of the SR-processed image increased by approximately 40% compared with those of the unprocessed image at a Nyquist frequency of approximately 3 cycle/mm of the 5-MP monitor (Fig. 5). Figure 6 presents the NPS of the 5-MP LCD monitor on which the X-ray exposed image of the ACR phantom is displayed at a pixel-by-pixel magnification. The overall NPS value of the SR-processed X-ray phantom image was slightly greater than that of the unprocessed image at frequencies higher than about 1 cycle/mm, whereas the noise levels of the overall NPS decreased gradually with an increasing spatial frequency. In addition, the overall NPS value of the displayed X-ray phantom image was 10^2 times greater than the inherent value of the 5-MP monitor, especially in the low-frequency range.

Based on the judgments of the four radiologists, the number of images (and the corresponding fractions [%]) selected as having better visibility for subtle microcalcifications owing to the SR function in 2-AFCSM were found to be 36 [80%], 37 [82%], 41 [91%], and 33 cases [73%] (averaging approximately 82%, with the 95% CI ranging from 70 to 93%). The fraction of SR-processed images selected as having better visibility for subtle microcalcifications in this dataset was statistically significant ($p < 0.001$) for the alternative hypothesis ("The SR-processed images have better visibility than the unprocessed images, i.e., the fraction >> 50%").

4 Discussion

This paper presented the effects of image display application with the SR function on displayed images on a 5-MP mammography display monitor. The SR function was designed not to overemphasize the displayed images but to compensate for the spatial frequency amplitude due to the resolution limit of the monitor. This technique in accordance with the given physical performance of individual LCD monitors can be incorporated into existing display systems. The filters for SR processing were formed based on the ideal frequency response of the inverse of the measured monitor MTFs in the horizontal and vertical directions. The frequency responses of the filters with the restricted coefficients converged to the desired ones of the inverse of the monitor MTFs, with increasing filter size. Although the frequency response of the filter depended on the values of its coefficients and its matrix size, the filter coefficients were restricted to a matrix of size 5 × 5 to simplify the implementation of the SR-processing algorithm on workstations for medical use. Consequently, the actual frequency response approximated with the 5 × 5 filter coefficients used for the SR function deviated a little from the desired frequency response of the inverse of the measured monitor MTFs (Fig. 3).

Figures 4 and 5 demonstrate that the SR function contributes to sharpness enhancements in the digital image displayed on the 5-MP LCD monitor, especially at higher spatial frequencies, in accordance with the inverse frequency responses of the monitor MTF. As the SR function increases the relative signal intensities of the displayed image at higher spatial frequencies, it amplifies the high spatial frequency noise [10-13]. Thus, although the noise levels of the overall NPS decreased gradually with increasing spatial frequency, the increase in the image noise caused by SR processing was inevitable, especially at frequencies higher than approximately 1 cycle/mm (Fig. 6). These results suggest that there is still room for improvement in suppressing noise amplification using such filters as a Wiener filter [11].

Two approaches, that is, line and bar-pattern methods, were taken to measure the monitor MTFs, thereby making a minor difference of the resultant MTFs between the two, especially in the vertical direction [Fig. 2(b) vs. Fig. 5(b)]. We applied the line method recommended in Ref. [2] to measure the MTF monitor to design the filter for the SR function. However, the line method is not suitable for verifying the effectiveness of the SR function based on the amplitude enhancements of a 1-pixel line in the background area owing to the complicated processes of background removal from the line response functions. We used the bar-pattern method to experimentally demonstrate the effectiveness of the SR function on the MTF characteristics based on the amplitude enhancements of the square-wave profiles, while the measurable frequencies were restricted to only five points.

The sharpness enhancements induced by SR processing were subtle when bone fracture images displayed on a 3-MP monitor were interpreted [14]. In the present paper, to reflect the slight difference in the image sharpness between SR-processed and unprocessed mammographic images, we performed a 2-AFCSM of the clustered microcalcifications with a subtle contrast displayed on the 5-MP mammography monitors. It is assumed that the lower the pixel size of a display monitor, the greater the enhancement effect on the displayed radiographic images provided by the SR-processing algorithm because of the increased Nyquist frequency of the monitor. Furthermore, the sharpness enhancement effects induced by SR processing would be more sensitive in a reduced magnification because the frequency ranges of the dominant components in the clustered microcalcifications would shift toward the higher-frequency ranges. Although the observers were blinded to the right/left location of the SR-processed or unprocessed images displayed on the two LCD monitors, most SR-processed images (approximately 82%) were found to have a superior visibility for interpreting clustered microcalcifications.

Our observer performance data indicate that the SR function promises improved visibility of subtle microcalcifications on digital mammograms, particularly when they are displayed on the 5-MP mammography monitor at a reduced magnification. However, the results obtained in our retrospective study may be limited because only a small number of specific cases was considered. Although a 2-AFC method is sensitive to differences between two similar images [20], our 2-AFC design with the ROI does not indicate that the SR function helps improve the diagnostic accuracy of mammography in clinical practice. Therefore, additional experiments need to be conducted to verify the detection performance for the microcalcifications. Further validation is required for cases with different types of microcalcifications and/or with different display magnifications. In addition, other types of lesions or medical images such as chest radiographs, bone radiographs, and computed tomographic images, need to be interpreted.

5 Conclusion

The image display application with the SR function described in this paper enhanced the image sharpness displayed on a 5-MP mammography LCD monitor based on the deficiencies in the monitor MTF with a certain increase in the image noise. The SR-processing algorithm, which promises the optimal representation of LCD monitors, has the potential to improve the observer performance of radiologists, particularly when reading subtle microcalcifications on digital mammograms. However, further observer studies must be performed to demonstrate the clinical utility of SR-processed images displayed on LCD monitors in improving the observer performance for the diagnosis of digital radiographic images.

References

1. Kagadis GC, Walz-Flannigan A, Krupinski EA, Nagy PG, Katsanos K, Diamantopoulos A, Langer SG (2019) Medical imaging displays and their use in image interpretation. Radiographics 33(1):275-291. https://doi.org/10.1148/rg.331125096
2. Samei E, Badano A, Chakraborty D, Compton K, Cornelius C, Corrigan K, Flynn MJ, Hemminger B, Hangiandreou N, Johnson J, Moxley M, Pavlicek P, Roehrig H, Rutz L, Shepard J, Uzenoff R, Wang J, Willis C (2014) Assessment

of display performance for medical imaging systems: Executive summary of AAPM TG18 report. Med Phys 32(4):1205-1225. https://doi.org/10.1118/1.1861159

3. Fan J, Roehrig H, Sundareshan MK, Krupinski EA (2006) Noise estimation and reduction on five medical liquid-crystal displays. J Soc Inf Disp 14(10):861-866. https://doi.org/10.1889/1.2372419
4. Ichikawa K, Kodera Y, Nishimura A, Hasegawa M, Kimura N, Takemura A, Matsubara K (2008) Analysis method of noise power spectrum for medical monochrome liquid crystal displays. Radiol Phys Technol 1(2):201-207. https://doi.org/10.1007/s12194-008-0029-y
5. Ichikawa K, Hasegawa M, Kimura N, Kawashima H, Kodera Y (2008) A new resolution enhancement technology using the independent sub-pixel driving for the medical liquid crystal displays. IEEE J Display Technol 4(4):377-382. https://doi.org/10.1109/jdt.2008.922414
6. Tokurei S, Morishita J (2015) A method for evaluating image quality of monochrome and color displays based on luminance by use of a commercially available color digital camera. Med Phys 42(8):4773–4782. https://doi.org/10.1118/1.4926850
7. Giger ML, Doi K (1984) Investigation of basic imaging properties in digital radiography. I. Modulation transfer function. Med Phys 11(3):287-295. https://doi.org/10.1118/1.595629
8. Sivaramakrishna R, Obuchowski NA, Chilcote WA, Cardenosa G, Powell KA (2000) Comparing the performance of mammographic enhancement algorithms. AJR Am J Roentgenol 175(1):45-51. https://doi.org/10.2214/ajr.175.1.1750045
9. Pisano ED, Cole EB, Hemminger BM, Yaffe MJ, Aylward SR, Maidment AD, Johnston RE, Williams MB, Niklason LT, Conant EF, Fajardo LL, Kopans DB, Brown ME, Pizer SM (2000) Image processing algorithms for digital mammography: a pictorial essay. Radiographics 20(5):1479-1491. https://doi.org/10.1148/radiographics.20.5.g00se311479
10. Reiker GG, Blume HR, Slone RM, Woodard PK, Gierada DS, Sagel SS, Jost RG, Blaine GJ (1997) Filmless digital chest radiography within the radiology department. Proc SPIE 3035:355-368. https://doi.org/10.1117/12.274591
11. Roehrig H, Dallas WJ, Krupinski E, Fan J, Chawla A, Gandhi K (2003) Display of mammograms on a CRT. In: Peitgen HO (ed) Digital mammography, Springer, Berlin, 452-454. https://doi.org/10.1007/978-3-642-59327-7_107
12. Krupinski EA, Roehrig H, Engstrom M, Johnson J, Lubin J (2003) MTF correction for optimizing softcopy display of digital mammograms: Use of a vision model for predicting observer performance. Proc SPIE 5034:323-327. https://doi.org/10.1117/12.479980
13. Krupinski EA, Johnson J, Roehrig H, Engstrom M, Fan J, Nafziger J, Lubin J, Dallas WJ (2003) Using a human visual system model to optimize soft-copy mammography display: influence of MTF compensation. Acad Radiol 10(9):1030-1035. https://doi.org/10.1016/s1076-6332(03)00293-9
14. EIZO Corporation. Study to demonstrate efficiency of sharpness recovery. White Paper. https://www.eizo.co.jp/support/db/files/technical_information/2016/Q16B014-AS-07001.pdf. Accessed 7 Aug 2020.
15. Miller TR, Sampathkumaran KS (1982) Design and application of finite impulse response digital filters. Eur J Nucl Med 7(1):22-27. https://doi.org/10.1007/bf00275240
16. Ichikawa K, Kodera Y, Fujita H (2006) MTF measurement method for medical displays by using a bar-pattern image. J Soc Inf Disp 14(10):831-837. https://doi.org/10.1889/1.2372416
17. Ichikawa K, Nishi Y, Hayashi S, Hasegawa M, Kodera Y (2008) Noise reduction effect in super-high resolution LCDs using independent sub-pixel driving technology. Proc SPIE 6917: 69171F. https://doi.org/10.1117/12.770848
18. Shiraishi J, Abe H, Ichikawa K, Schmidt RA, Doi K (2010) Observer study for evaluating potential utility of a super-high-resolution LCD in the detection of clustered microcalcifications on digital mammograms. J Digit Imaging 23(2):161-169. https://doi.org/10.1007/s10278-009-9192-x

19. Ihori A, Fujita N, Sugiura A, Yasuda N, Kodera Y (2013) Phantom-based comparison of conventional versus phase-contrast mammography for LCD soft-copy diagnosis. Int J Comput Assist Radiol Surg 8(4):621-633. http:// doi.org/10.1007/s11548-012-0805-3
20. Muramatsu C, Li Q, Schmidt RA, Shiraishi J, Suzuki K, Newstead GM, Doi K (2007) Determination of subjective similarity for pairs of masses and pairs of clustered microcalcifications on mammograms: comparison of similarity ranking scores and absolute similarity ratings. Med Phys 34(7):2890-2895. http:// doi.org/10.1118/1.2745937

Table Caption

Table 1 Inverse filter coefficients with a restricted size of 5 × 5, calculated from the inverse of the measured MTFs in the horizontal (non-subpixel) and vertical (subpixel) directions of the 5-MP mammography LCD monitor

Figure Captions

Fig. 1 Pixel structure of two 5-MP monochrome LCD panels (pixel size: 0.165 mm) with different pixel aperture ratios: (a) A conventional panel with a pixel aperture ratio of 33.0% and (b) a higher-luminance panel with a pixel aperture ratio of 41.7% used in this study. Each pixel in a monochrome LCD monitor is composed of three subpixel elements (separated by dashed lines). Note that the "black matrix area" means the inactive area created in the manufacturing process to prevent light leakage from the backlight of the LCD panels.

Fig. 2 (a) MTFs and (b) NPS in the horizontal (non-subpixel) and vertical (subpixel) directions of the 5-MP monochrome LCD monitor

Fig. 3 Two types of frequency responses of the finite impulse response (FIR) inverse filters in the horizontal (H) and vertical (V) directions of the LCD monitor; solid lines indicate the desired responses calculated from the inverse of the monitor MTFs and the dashed lines indicate the ones implemented with 5 × 5 filter coefficients

Fig. 4 (a) A partial image of the captured horizontal bar-pattern image including the five bars with 1-, 2-, 3-, 4-, and 6-pixel widths displayed on the 5-MP monochrome LCD monitor. Square-wave profiles of the five bars with three-pixel width corresponding to approximately 1.0 cycle/mm in the (b) horizontal and (c) vertical directions, obtained from the area bounded by the dashed line of the SR-processed and unprocessed bar-pattern images.

Fig. 5 MTFs in the (a) horizontal and (b) vertical directions measured from the square-wave profiles of the SR-processed and unprocessed bar-pattern images displayed on the 5-MP monochrome LCD monitor

Fig. 6 The NPS in the (a) horizontal and (b) vertical directions measured from the X-ray exposed image of the ACR accreditation phantom (for overall NPS) and uniform pattern image (for inherent NPS), displayed on the 5-MP monochrome LCD monitor, respectively. The overall NPS value of the SR-processed X-ray phantom image was slightly greater than that of the unprocessed one, especially at frequencies higher than about 1 cycle/mm.

Acknowledgments

The authors are grateful to Kenshi Shiotsuki, RT for useful discussions, Takafumi Nomura, MD, Keisuke Miyoshi, MD, Shoko Ariyoshi, MD, and Masaki Kamiya, MD (Yamaguchi University) for their participation as observers, Sono Kanoya, RT, Fumiko Yurino, RT, Ayumi Hashimoto, RT, and Eri Tokurei, RT for their assistance in the preparation of

a database containing clinical digital mammograms, Mamoru Ogaki, Yusuke Bamba, Masaki Kita, and Noriyuki Hashimoto (EIZO Corporation) for the technical support on display monitors with image processing systems, and Kazuyuki Watanabe, Kazushige Hatori, and Hideaki Mizobe (Canon Corporation) for providing a single-lens reflex digital color camera.

Declarations

Funding This work was supported in part by grant from EIZO Corporation (Ishikawa, Japan).

Conflicts of interest/Competing interests J. Morishita received a research grant from EIZO Corporation (Ishikawa, Japan).

Ethics approval All procedures in studies involving human participants were performed in accordance with the ethical standards of the Institutional Review Board and with the 1964 Helsinki Declaration and its later amendments, or comparable ethical standards.

Consent to participate Informed consent was waived for the all images used in this study by the Institutional Review Board.

Consent for publication Not applicable

Availability of data and material Not applicable

Code availability Not applicable

Fig. 1

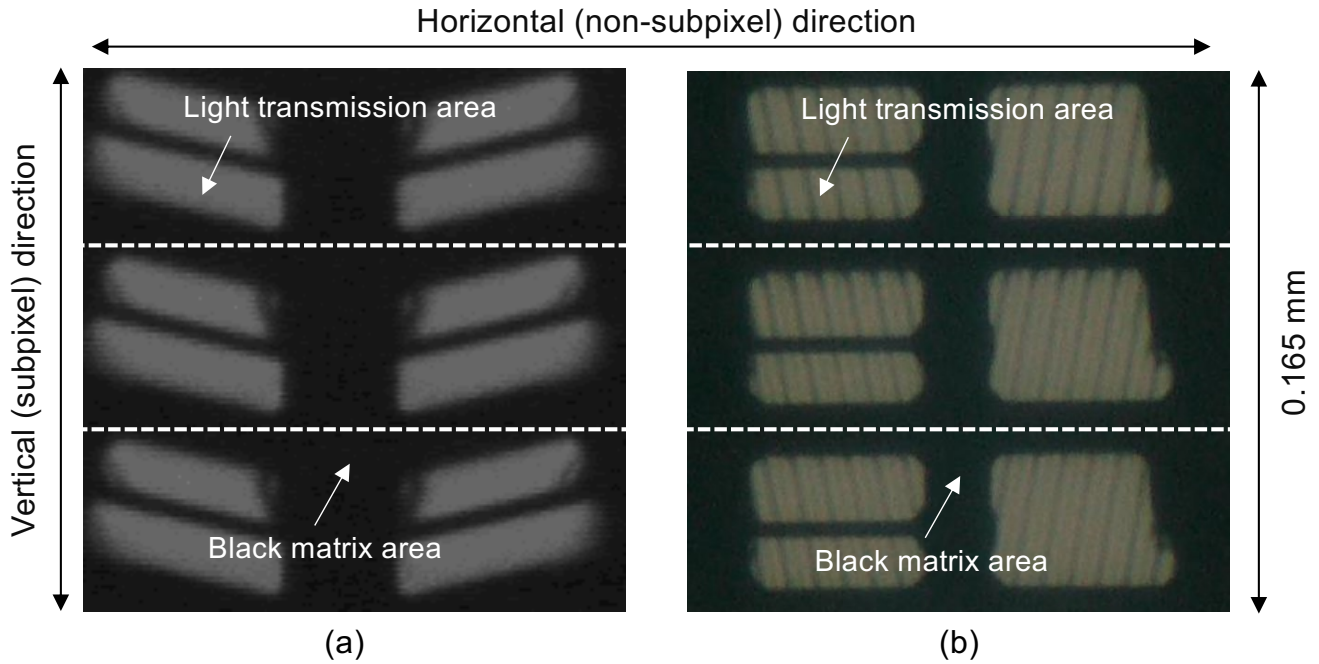
Horizontal (non-subpixel) direction
Vertical (subpixel) direction
Light transmission area
Black matrix area
Light transmission area
Black matrix area
0.165 mm
(a)
(b)

Fig. 2

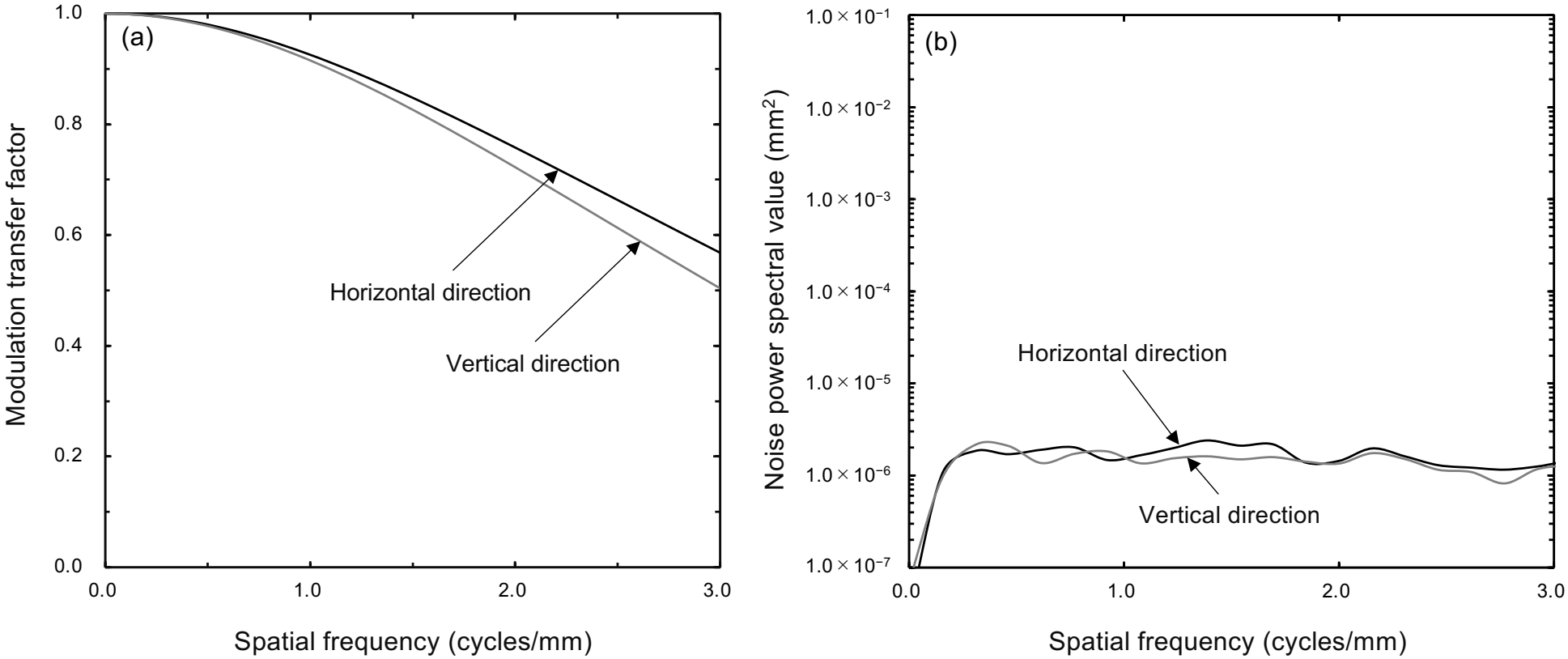
(a)
Modulation transfer factor
1.0
0.8
0.6
0.4
0.2
0.0
Horizontal direction
Vertical direction
0.0
1.0
2.0
3.0
Spatial frequency (cycles/mm)
(b)
Noise power spectral value (mm²)
1.0 × 10⁻¹
1.0 × 10⁻²
1.0 × 10⁻³
1.0 × 10⁻⁴
1.0 × 10⁻⁵
1.0 × 10⁻⁶
1.0 × 10⁻⁷
Horizontal direction
Vertical direction
0.0
1.0
2.0
3.0
Spatial frequency (cycles/mm)

Fig. 3

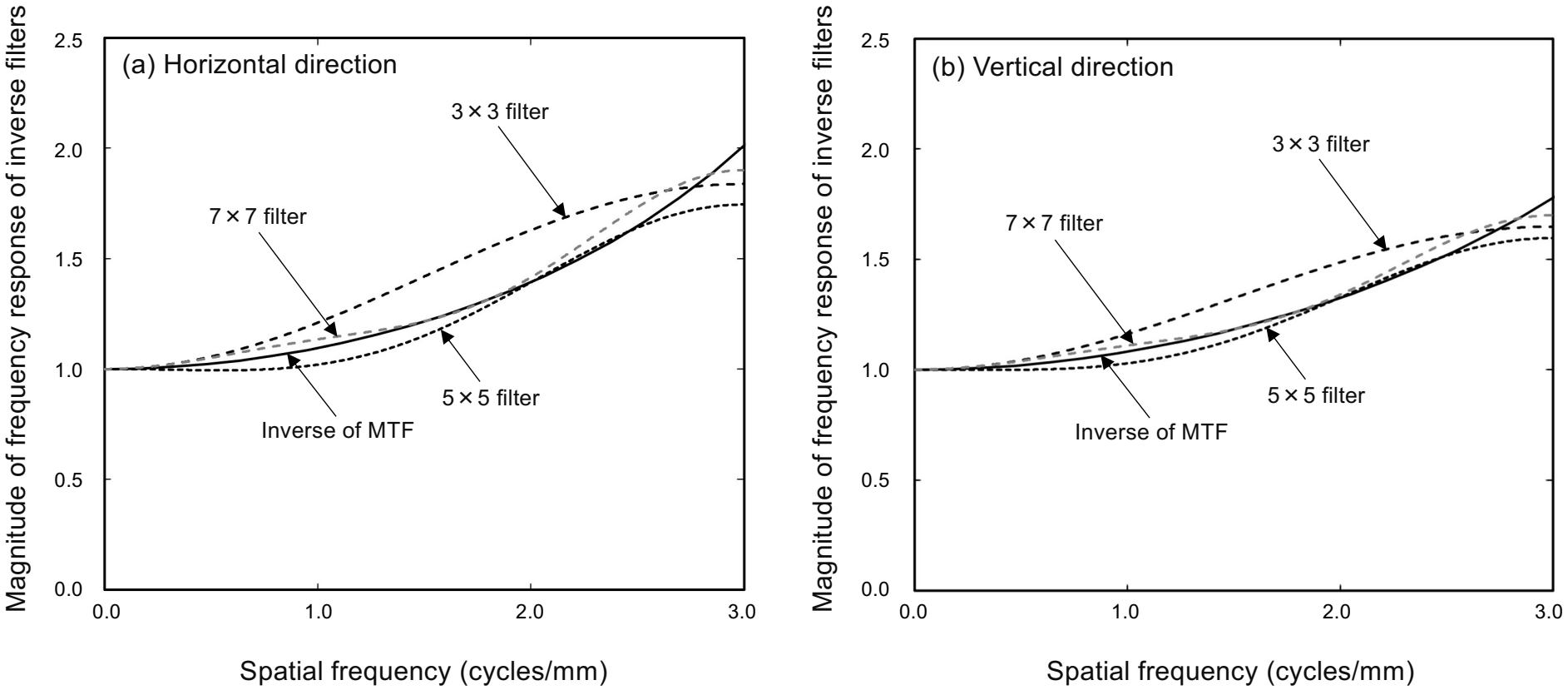
(a) Horizontal direction
3 × 3 filter
7 × 7 filter
5 × 5 filter
Inverse of MTF
Magnitude of frequency response of inverse filters
Spatial frequency (cycles/mm)
0.0
0.5
1.0
1.5
2.0
2.5
3.0
(b) Vertical direction
3 × 3 filter
7 × 7 filter
5 × 5 filter
Inverse of MTF
Magnitude of frequency response of inverse filters
Spatial frequency (cycles/mm)

Fig. 4

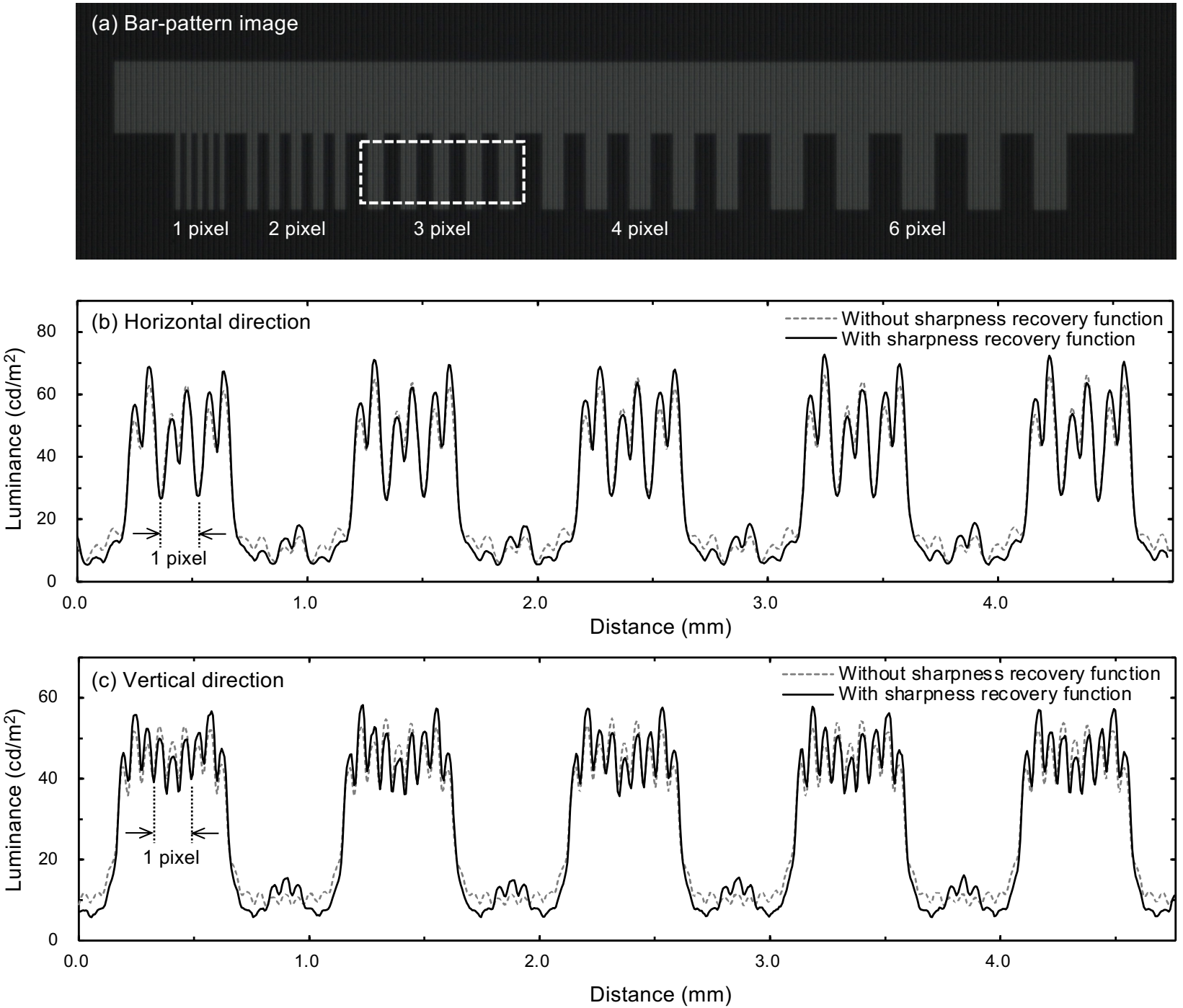
(a) Bar-pattern image
1 pixel
2 pixel
3 pixel
4 pixel
6 pixel
(b) Horizontal direction
Without sharpness recovery function
With sharpness recovery function
Luminance (cd/m2)
1 pixel
Distance (mm)
(c) Vertical direction
Without sharpness recovery function
With sharpness recovery function
Luminance (cd/m2)
1 pixel
Distance (mm)

Fig. 5

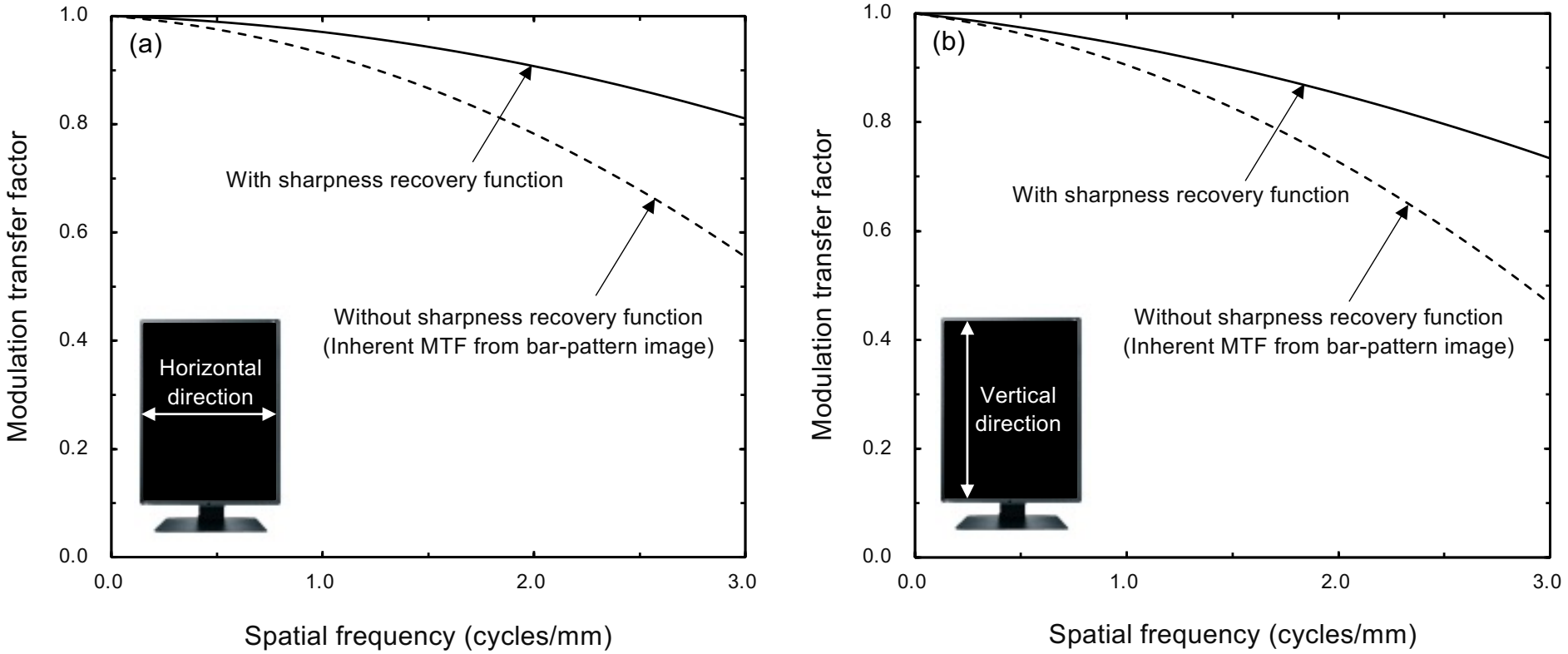
(a)
Modulation transfer factor
1.0
0.8
0.6
0.4
0.2
0.0
0.0
1.0
2.0
3.0
Spatial frequency (cycles/mm)
With sharpness recovery function
Without sharpness recovery function
(Inherent MTF from bar-pattern image)
Horizontal
direction
(b)
Modulation transfer factor
Spatial frequency (cycles/mm)
With sharpness recovery function
Without sharpness recovery function
(Inherent MTF from bar-pattern image)
Vertical
direction

Fig. 6

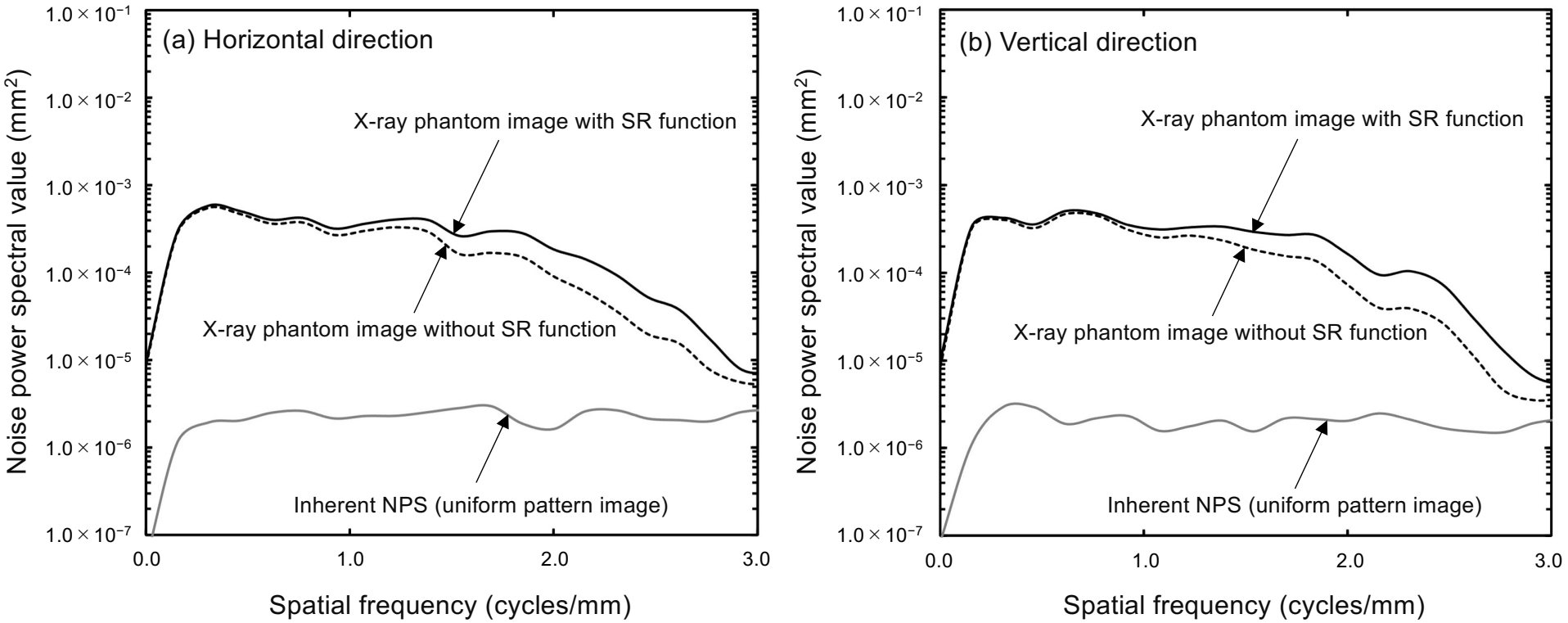
(a) Horizontal direction
(b) Vertical direction
X-ray phantom image with SR function
X-ray phantom image without SR function
Inherent NPS (uniform pattern image)
Noise power spectral value (mm²)
Spatial frequency (cycles/mm)
1.0 × 10⁻¹
1.0 × 10⁻²
1.0 × 10⁻³
1.0 × 10⁻⁴
1.0 × 10⁻⁵
1.0 × 10⁻⁶
1.0 × 10⁻⁷
0.0
1.0
2.0
3.0